Moor Journal of Agricultural Research 23: 11 – 27, 2022

MOOR JOURNAL OF AGRICULTURAL RESEARCH

Land Use Types Influence Diffuse N and P Entering a River in an Agricultural Watershed: Evidence from Compound-Specific Stable Isotope

[1]*Are, K.S., [2]Guo, H. and [2]Li, Y

[1]Institute of Agricultural Research and Training, Obafemi Awolowo University, Moor Plantation, Ibadan.

[2]Key Laboratory of Agro-Environment and Agro-Product Safety, Guangxi University, 530004, Nanning, China

Correspondence: kayodeare@gmail.com; +234-8035721035

Keywords

Carbon-13 ($\delta^{13}C$)
Fatty acids
Soil proportion
Entry coefficient
Rainfall season

Abstract

The increase in sediment and nutrient losses to freshwater has resulted in ecosystem degradation and non-point source (NPS) pollution worldwide. Using stable isotopes and direct monitoring techniques to quantify the losses has been effective, but it has received little scientific attention. This study identified and quantified the sources of sediment, particulate nitrogen (PN), and phosphorus (PP) entering rivers from land use types, and clarified their influencing factors. Compound-specific stable isotope (CSSI), using the carbon-13 ($\delta^{13}C$) isotope signature of fatty acids, was applied in June and September 2019. Four sediment sources: eucalyptus, road, sugarcane, and stream channel, were identified in the watershed. The $\delta^{13}C$ of the sediment mixtures was -16.80 and 17.01 ‰ in June and September, respectively. The soil proportions from different sources in June and September were in the order of road (37.1%) >sugarcane (32.4%) >stream channel (27.5%) >eucalyptus (3.1%), and sugarcane (40.5%) >stream channel (29.2%) >road (27.6%) >eucalyptus (2.7%), respectively. Ground cover, soil organic matter (SOM), bulk density, and slope gradient significantly (P <0.05) influenced sediment, PN, and PP entering the river. The combined application of CSSI and Bayonet monitoring techniques could provide a better understanding of sediment and nutrient redistribution in agricultural watersheds.

Introduction

Soil erosion has been a major global problem with its current rates standing at 43 Pg yr^{-1}, constituting a treat to land, ecosystem services, and degradation of downstream water quality (Borelli *et al*., 2020). The intensification of soil erosion and nutrient losses has been linked to anthropogenic activities that involved land use changes, which influence a range of important soil functions and contribute to surface water pollution (Recanatesi *et al*., 2013; Zhou *et al*., 2019). In recent past, most studies focused on direct contribution of a land use type to sediment and associated-nutrient losses to waterbodies. However, land use alone cannot explain the quantities of pollutants and their delivery to freshwaters, since configurations within the same land use could modify the dynamics of the exports by soil erosion and estimation of exported nutrient loads. Therefore, accurate measurement of pollutants reaching freshwaters from a particular land use type is germane to determine its specific contribution to NPS pollution.

The change of land use mode, especially the reclamation of forest-grass land, has led to increase in soil erosion, having significant impact on soil environment and non-point source pollution of water in a catchment (Recanatesi *et al*., 2013; Tiecher *et al*., 2017). However, not all the eroded sediment and associated nutrients are transported into the river as some are stacked in the low-lying area, while only a fraction goes to the surface water system

via erosion channels. The transportation of these sediment and associated nutrients from farmlands are influenced by topography, soil, rainfall, the connectedness of land use, hydrology and other factors, with high spatial and temporal variability (Du and Wailing, 2017; Li *et al*., 2020a). This has made it difficult to identify the sources of sediment in the waterbodies, and quantify the specific contribution to river sediment and associated PN and PP by different land use types. But the determination of entry coefficient of exported loads (a measure of definite quantity of pollution reaching freshwaters from different sources) through combine application of CSSI and online Bayonet monitoring of channel erosion may alleviate the difficulty and forestall overestimation of exported nutrient loads.

The need for a reliable information on the principal sources of sediment and associated nutrients has resulted in employing different techniques for their estimations. Techniques such as the traditional monitoring of watershed-based erosion and sediment redistribution measurements, aerial photographs, satellite imagery analysis, erosion modeling and tracking of geochemical properties have been employed (Collins *et al*., 1997; Evrard *et al*., 2013; Collins *et al*., 2017). Estimating sources delivering sediment to the river network by these conventional methods are difficult, costly, and time-consuming, and some of them only measure sediment deposition rates without considering the changes in the configurations within the source area. However, linking land-use fingerprints to sediments in the deposition belt has proved to be an effective technique for identifying sources of eroded sediment, and areas prone to channel erosion. Isotopic techniques are now emerging as an affordable alternative tool for assessing soil erosion, both temporally and spatially, and to identify areas susceptible to soil erosion (Walling, 2005, 2008; Claudio *et al*., 2018). Stable isotope tracer technique of monomer compounds is an effective isotope identification method, which is often used for sediment source identification of different land use types (Reiffarth *et al*., 2016, 2019). A new stable isotope technique of Compound-Specific Stable Isotope (CSSI), a carbon-13 ($\delta^{13}C$) stable isotope signature of fatty acids that was first used on estuarine sediments by Gibbs (2008), although not used for channel erosion, is effective to distinguish and apportion the contemporary soil sources contribution to pollution from different land uses (Mabit *et al*., 2018; Claudio *et al*., 2018). Since the plant species in a defined land area produce organic compounds that seep into the soil from roots and leaves, it is easier for isotopic signatures of soil from a particular land use to be identified. Although, the range of organic compounds produced by different plant species is similar, however, ^{13}C ($^{13}C/^{12}C$) values are different for plant species (Gibbs, 2008; Tolosa *et al*., 2013). At present, CSSI biometric fingerprint technology has been widely used conveniently for sediment tracing, but it is seldom used for studies in agricultural ecosystems with different land use types (Reiffarth *et al*., 2016; Upadhayay *et al*., 2017) and agricultural hillslopes prone to channel erosion.

Previous study by Jin *et al*. (2020) highlighted the contributions of anthropogenic activities to diffuse nutrient pollution using soil radiotracers (i.e., ^{7}Be, ^{137}Cs, $^{210}Pb_{ex}$) and fingerprints (such as stable isotopes of $\delta^{15}N$, $\delta^{18}O$) for the identification of land-use-specific nutrient source. However, neither the soil radiotracers nor fingerprints of stable isotopes could precisely provide information on land-use-specific sediment sources of soil accumulated and deposited along a landscape (Alewell *et al*., 2016; Mabit *et al*., 2018). But these shortcomings could be addressed by CSSI signatures as effective isotopic fingerprinting approach for land-use-specific sediment source identification (Reiffarth *et al*., 2016). Therefore, this study was aimed at using compound-specific stable isotope (CSSI) techniques to: (i) quantify and apportion the different sediment

sources (roads, stream channels, sugarcane and eucalyptus fields) flowing to the river from agricultural watershed, (ii) determine the entry coefficient of PN and PP entering river from different land use types following changes in ground cover between June and September 2019, and (iii) clarify the key influencing factors of sediment and nutrient losses from different land use types.

Materials and Methods

Study site

The study site is an agricultural watershed (107° 39′ E, 22° 20′ N), located in the upstream section of Kelan reservoir of Zuojiang river basin in Guangxi Zhuang Autonomous Region, China (Fig. 1). The watershed, which covers an area of 120 ha, is dominated by agricultural land, and it is an important sugarcane producing area in the region. Following implementation of land integration planning policy in Guangxi Zhuang autonomous region in 2018, approximately 74% of the watershed was cultivated with sugarcane, and 21% of the land use, mostly in the upper reaches, with eucalyptus production (Li *et al*., 2021). The remainder was occupied with road networks (4.5%) and stream channels (0.5%). The sugarcane growth period in the area spans from March at planting to December/January at harvesting. The land area has a rolling topography with an average gradient of about 35 %. The predominant form of erosion in this area is channel erosion because of the topography. The area belongs to a humid subtropical climate with annual temperature ranging from 13.8℃ in January to 28.1℃ in July. The average yearly precipitation reaches 1400 mm with 130–200 raining days mainly distributed from March to September. The precipitation from June to September accounts for about 61% of the total precipitation. Specific details regarding the study area lithology, soil, slope gradients, land cover and agricultural activities had been presented in Li et al. (2020a, 2020b, 2020c).

Collection of suspended sediment

The study area comprised three dendritic-shaped sub-watersheds: S1, S2 and S3, based on topographic directions and drainage areas, where runoff-sediment monitoring stations were installed (Fig. 1). To characterize the eroded sediment from the watershed, automatic water and sediment sampling devices (ISCO 6712, USA) were installed at sub-watersheds outlets (monitoring stations), to collect water-sediment mixture passing through the channels from the river bed during rainfall events. Detailed information regarding the water-sediment mixture collection and measurements of suspended sediment during rainfall events were presented in Li et al. (2020a). The sediment concentration for each rainfall event was estimated in the laboratory after drying the sediment samples for 24 h at 45ºC. The dried sediment samples were allowed to pass through 0.149 mm sieve for the determination of sediment-associated nitrogen (N) and phosphorus (P) concentration during rainfall events. In order to apportion the sediment sources to samples collected in June and September by CSSI analysis, a composite sediment sample was prepared by mixing all individual samples from the monitoring stations following Gibbs (2014) protocols.

Field measurements and soil sampling from different land use types

Details about the distribution of the land use types were reported by Li et al. (2021). Spatially-integrated soil samples were collected from a total of four different land uses (i.e., roads (unpaved), stream channels, sugarcane and eucalyptus fields), which were considered as potential contributors to the sediment sources to river within the watershed. Using 10 cm diameter hand core samplers, the soil samples were collected from the areas that are potentially vulnerable to channel erosion at 0–2 cm in most locations, and 0–5 cm depth where the erosion degree required deeper sampling depth. At the same time, a cylindrical core of 5 cm in height and diameter was used to collect surface soil for bulk density following a procedure similar to the

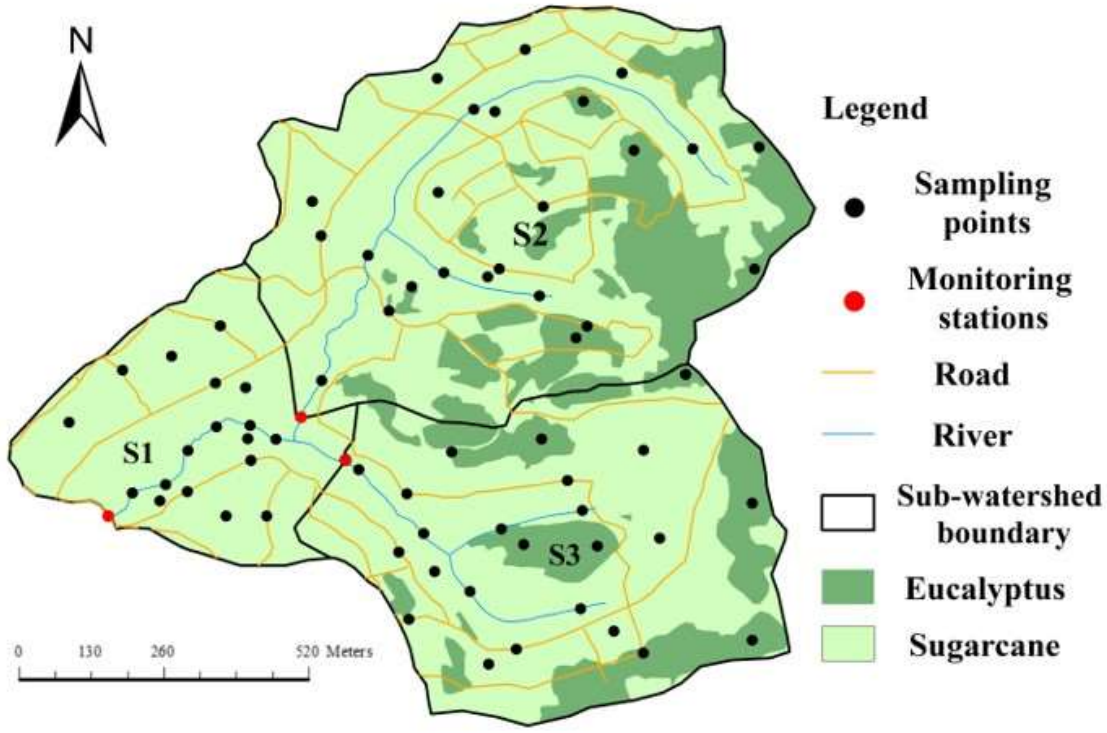

Fig.1. Sampling location showing different land use types and sampling points within the watershed. S1, S2 and S3 represents sub-watersheds within the watershed

one in Grossman and Reinsch (2002).

For sugarcane and eucalyptus fields, we sampled at 10 m interval from the first in grid pattern to obtain about 8–13 soil samples, which were thoroughly mixed in a bucket to provide composite samples. For the roads, the samples were collected specifically from the locations where there were sediment depositions, to ensure that only sediments from the road were sampled. For the stream channels, the spatially-integrated samples of the stream channel sediment were collected from the channel banks at the top 0–5 cm depth. All sampling points were georeferenced by using a global positioning system (GPS, Trimble Juno 3E). At each point, where present, the leaf litters, stones and roots were removed before soil sampling. For each land use, at least 6 representatives of spatially-integrated well mixed composite samples were collected for CSSI analysis. The samples were placed in zip-lock bags, labelled accordingly and transported to the laboratory for further analyses.

Quantification of sediment and particulate nutrients entering river channels

Automatic water and sediment samples were set at a liquid level trigger sampling mode at the outlets of the sub-watersheds during each rainfall events to measure volume of runoff. The sediment loss rate (S_L, t ha^{-1}) for each rainfall event was obtained following Eq. (1):

$$S_L = \sum_{i=1}^{n} \frac{S_{ci} * V_i * T_i}{A_x * 10^3} \quad (1)$$

where n is the total number of samples, i is the individual sample per rainfall event, S_{ci} is the suspended sediment concentration (g m^{-3}), V_i is the runoff volume at different sampling periods (m^3 hr^{-1}), T_i is the sampling interval time of different samples (hr), and A_x is the sub-watershed area (ha) that contributed to the sediment in each outlet.

For each rainfall event, the subsample of the dried sediment was examined for sediment-associated N and P using standard methods. The sediment-associated N concentration (g kg^{-1}) was determined following Kjeldahl method as described by Bremner (1996) while the

sediment-associated P concentration (g kg^{-1}) was determined colorimetrically using a hot perchloric acid digestion (Sommers and Nelson, 1972). The magnitudes of N and P losses (kg ha^{-1}) for each rainfall event were calculated as follow in Eq. (2):

$$N_L \text{ or } P_L = \sum_{i=1}^{n} \frac{S_{ci} * V_i * T_i * N_i / P_i}{A_x} \quad (2)$$

where, N_L or P_L is the sediment-associated N or P loss (kg ha^{-1}),, N_i/P_i is the concentration of sediment-associated N or P (g m^{-3}).

The entry coefficients (E_c) of PN and PP entering river channels were estimated following Eq. (4)

$$E_c = \lambda * \frac{Q_{LU}}{Q_A} \quad (3)$$

where λ ($0 \leq \lambda < 1$) is the nutrient contribution of a source by proportion; Q_{LU} is the exported nutrient from a particular land use type (kg ha^{-1}) while Q_A is the exported nutrient from the entire watershed (kg ha^{-1}).

CSSI samples pre-treatment and analysis

The CSSI analysis was conducted using a modified Gibbs (2008; 2014) protocols. For the extraction of fatty acids (FAs), 20 g of soil samples was mixed with diatomite powder (soil sample + diatomite 4:1) and then loaded in the extraction pool of an Accelerated Solvent Extractor (ASE 350), 30–50 ml of pure dichloromethane (DCM) was added as solvent to ensure that more FAs are extracted. The samples were heated to 100 °C and then compressed to 2000 psi for 15 mins. The extract was transferred to 100-ml pear-shaped flask, placed on a rotary evaporator and steamed at 34 °C. Using Pasteur pipette, the extract in the pear-shaped flask was transferred to a 20 ml test tube with the pear-shaped flask thoroughly rinsed with n-hexane to the test tube, and then evaporated to near dryness in a fume hood (at 40°C in water bath). 5 ml of a saponified solution was added to the extract in a long test tube and placed in a water bath (at 60°C) overnight (about 12 h). 1 ml of concentrated HCl (pH <2) was added to the mixture and then mixed with Vortex mixer for 1 min and allowed to stand for 30 mins. Thereafter, 5 ml of n-hexane/DCM (93:7) was added, oscillated for 1 min, and then allowed to stand for 30 mins. This process was repeated 5 times with successive standing times reduced by 5 mins. The extract was transferred to a 100 ml pear-shaped flask and then evaporated off to about 1 ml by steaming at 38 °C. The extract was then filtered to a 10 ml Kimax screw-cap reaction tube through a column lined at the bottom with absorptive cotton and 3-5 cm of the column was filled with anhydrous Na_2SO_4 to remove impurities. The extract in the Kimax tube was then evaporated off by warming to 40°C under a slow stream of nitrogen gas to about 2 ml.

The composition and content of fatty acids (FAs) were measured with an Agilent 6890 GC gas chromatograph coupled to a Thermo-MAT 253 mass spectrometer through a GC-C-III combustion interface. The fatty acid methyl ester (FAME) was determined using GC-IRMS with external standards of C14:0, C16:0, C18:0, C20:0, C22:0, C24:0, C26:0, C28:0 and C30:0 FAMEs at C16:1, C18:1 and C18:2.

Three results were obtained from the analyses in the laboratory for CSSI: (i) $\delta^{13}C$ and %C of the bulk sample (after acidification), (ii) $\delta^{13}C$ values of all FAs extracted from the sample and converted to FAMEs, and (iii) $\delta^{13}C$ of the methanol used in the derivation step to produce the FAMES. The FAME was measured at the same time as the methanol ^{13}C. The fatty acid $\delta^{13}C$ was calculated using a mass balance equation:

$$\delta^{13}C_{FA} = \frac{\delta^{13}C_{FAME} - (1-X)\delta^{13}C_{Methanol}}{X} \quad (4)$$

where FA is the fatty acid under investigation, X is the fractional contribution of carbon atoms in the FA to the FAME. X was calculated from the number of carbons in the FA molecule divided by the number of carbon atoms in the FAME derived from the FA.

Mixing model for apportioning sediment

sources contribution and statistical analysis

The apportionments of source contribution to the sediment mixture during rainfall events were evaluated and compared using isotopic mixing models (Phillips and Gregg, 2001; 2003). In this study, we applied the IsoSource mixing model to establish isotopic proportions of sediment sources in the sediment mixtures in June and September 2018. According to Gibbs (2008) and Alewell *et al*. (2016), IsoSource is a linear model often used in agro-environmental studies, and it is based on the carbon content of each source soil. The model can accommodate many sources, but requires a minimum of 3 sources (Gibbs 2014). To use this model, data of corrected CSSI $\delta^{13}C$ values of the FAs from the source soils (roads, stream channels, sugarcane and eucalyptus fields) and the sediment mixture collected at the outlets were collated. The conversion of isotopic proportions into source soil proportions were determined as presented in Gibbs (2014) using Eq. (6):

$$\%Source_n = \left\{ \frac{{}^{I_n}/_{\%C_n}}{\sum_n^1 \left({}^{I_n}/_{\%C_n}\right)} \right\} * 100 \qquad 6)$$

where I_n is the mean feasible isotopic proportion of source soil *n* in the mixture as estimated from isotopic values of carbon by IsoSource, and $\%C_n$ is the % carbon in the source *n* soil.

Statistical analyses on data obtained from CSSI data were carried out using Origin® 2018b (OriginLab Corporation, Northampton, MA 01060, US). Identification of suitable FAs were determined using one-way analysis of variance (ANOVA), correlation analysis and polygon analysis (Phillips and Gregg, 2003). The mean values of the sediment proportions in June and September were separated using Turkey's honest significant difference (HSD) at $\alpha \leq 0.05$. A multivariate statistical approach with principal component analysis (PCA) was applied to identify the key underlying factors controlling sediment and associated nutrient losses from different land uses.

Results and Discussion

Determining the most appropriate fatty acids to identify the sediment sources

The isotopic values ($\delta^{13}C$-FA) and bulk soil organic carbon for different sediment sources and the mixtures in June and September are summarized in Tables 1 and 2. The isotopic $\delta^{13}C$ values of the C14:0 to C30:0 FAs showed relatively large differences between different land use soils, and exhibited both isotopic enrichment and depletion across all sources and mixture during June and September (Table 1). As suggested by Mabit *et al*. (2018), we chose the FAs that are only plant-specific, present in all sources and at a concentration level for accurate isotopic discrimination.

Table 1: Bulk $\delta^{13}C$ signatures and SOC of different FAs from four soil sources and the sediment mixture in June and September 2019

	Eucalyptus		Road		Sugarcane		Channel		Mixture	
FAs (in $\delta^{13}C$ ‰)	June	Sept	June	Sept	June	Sept	June	Sept	June	Sept
Myristic acid (C14:0)	-28.82	-30.25	-23.60	-22.66	-23.43	-24.36	-24.76	-23.65	-23.81	-24.60
Palmitic acid (C16:0)	-26.57	-26.65	-21.80	-21.50	-21.94	-20.92	-24.62	-20.87	-22.01	-24.07
Stearic acid (C18:0)	-23.58	-24.19	-22.41	-21.64	-22.31	-22.56	-24.20	-21.21	-22.02	-23.99
Arachidic acid (C20:0)	-21.18	-21.23	-19.84	-18.58	-20.80	-19.74	-21.07	-21.11	-21.50	-20.84
Behenic acid (C22:0)	-27.19	-27.54	-22.68	-21.65	-22.74	-21.86	-23.81	-23.09	-23.51	-22.30
Lignoceric acid (C24:0)	-30.75	-29.37	-23.30	-22.51	-23.21	-22.44	-24.63	-25.37	-24.32	-23.56
Hexacosoic acid (C26:0)	-32.41	-31.88	-23.21	-23.78	-23.79	-23.62	-26.36	-28.18	-25.78	-27.61
Octacosanoic acid (C28:0)	-32.03	-31.65	-22.18	-23.55	-24.71	-23.76	-24.87	-28.69	-25.03	-26.93
Triacontanoic acid (C30:0)	-31.98	-31.26	-21.05	-21.93	-23.45	-25.29	-25.20	-27.13	-24.17	NA

Table 2 Bulk soil organic carbon information of the land use types and sediment mixture in June 2019 and September 2019.

	$\delta^{13}C$ (‰)		C_{org} (%)	
Source	June	September	June	September
Eucalyptus	-21.71a	-21.12a	4.65a	4.42a
Road	-14.98b	-18.33a	1.05b	1.51a
Sugarcane	-15.97a	-16.57a	1.34b	1.74a
Channel	-17.78a	-17.30a	1.38a	1.38a
Mixture	-16.80a	-17.01a	0.99a	1.05a

Land use types followed by different letters for $\delta^{13}C$ and C_{org} values in June and September 2019 are significantly different by Turkey's HSD at $\alpha < 0.05$.

Using the analysis results in Tables 1 and 2, polygon analyses were performed to determine which FAs is/are most suitable to differentiate between the sources. The $\delta^{13}C$-FA value of the mixture should be within the mixed polygon formed by the source $\delta^{13}C$-FA. As shown in Figs. 2 and 3, only bulk soil organic carbon $\delta^{13}C$ and FAs C22:0 (Behenic acid) and C24:0 (Lignoceric acid) met the criteria and were suited for distinguishing between sediment sources. The results in Figs. 2 and 3 indicated that saturated long-chain FAs (C22:0 and FAs C24:0) are suitable to differentiate FAs' sources. Our findings are in congruence with the earlier findings of Alewell *et al*. (2016) and Mabit *et al*. (2018). As the chain length of fatty acids increases, the solubility decreases and the more the long-chain fatty acids are more stable than short-chain fatty acids (Upadhayay *et al*., 2017; Swales and Gibbs, 2020).

As shown in the mixing polygons of the two selected FAs, the bulk soil carbon $\delta^{13}C$ in all the biomarkers indicated strong identification ability (Fig. 3). The results of ANOVA demonstrated that the long-chain FAs (C20:0 – C30:0) differed significantly (P <0.001) among the four sources in June and September 2018. However, the short-chain FAs (C14:0 – C18:0) differed significantly (P<0.05) among the sources only in September but with no significant difference (P >0.05) in June 2018 (Table 1). On the other hand, the range of bulk soil $\delta^{13}C$ in the four sources was -21.71 ‰ to -14.98 ‰ with the sediment mixture values of -16.80 and 17.01 ‰ in June and September, respectively (Table 1). In June, the contribution of different sources to bulk soil $\delta^{13}C$ was in the order of road > sugarcane > channel > eucalyptus, but the contribution orders changed in September as: sugarcane > channel > road > eucalyptus. The comparison of the two months by the isotopic signatures showed that only the road exhibited significant difference (3.35‰, P <0.01) between June and September, but other sources did not show any significant differences. The significant reduction in $\delta^{13}C$ under the road may be attributed to increase in grasses growing on the roads and increased sugarcane canopy and leaf litters, which intercepted and reduced the erosive energy of runoff going to the adjacent roads.

Considering how the plants of the four sources are fixing carbon from atmospheric CO_2 during photosynthesis, they can be grouped into C_3 (grasses on road and stream channel and eucalyptus tree) and C_4 (sugarcane) plants. Generally, the range of $\delta^{13}C$ values in plant material varies from −10‰ to −34‰ with average C_3 and C_4 plants' values equal −27‰ and −13‰, respectively (Glaser, 2005). However, in our study, the average $\delta^{13}C$ values for C_4 plants were −15.97 and −16.57‰ in June and September 2018, which were significantly different from C_3 plants with -18.16 and -18.92 ‰ in the respective months. Similar to the work of Bravo-Linares *et al*. (2018), our study showed that C_3 plants are the main factor responsible for high negative $\delta^{13}C$ value in the watershed.

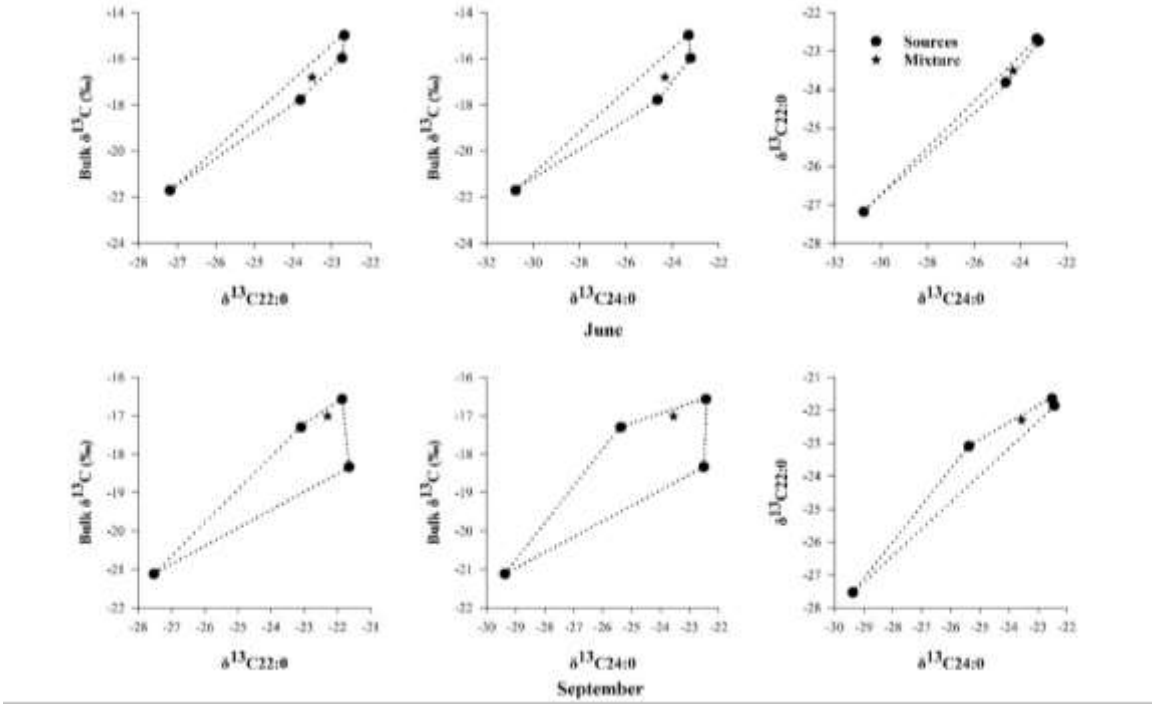

Fig. 2. Mixing polygons of selected FAs contributing to the mixture in June and September 2019

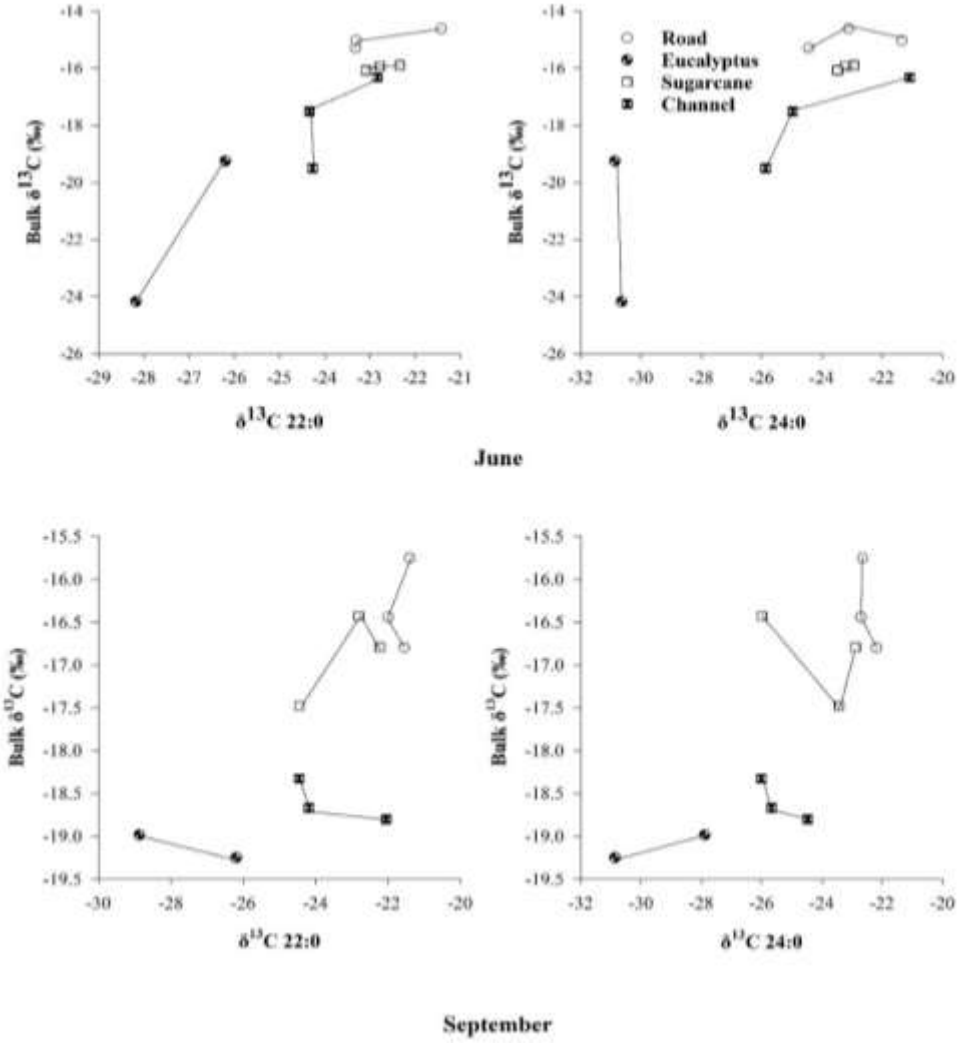

Fig. 3. Variability of the $\delta^{13}C$ signature of FAs (C22:0, C24:0) and bulk carbon of the soil sources in June and September 2019.

Before 2017, a large number of Eucalyptus (C_3 plant) was planted in the study watershed but replaced with sugarcane, showing that the typical high negative $\delta^{13}C$ value comes from C_3 plants (Table 2).

Proportions of soil contributed by different sources in the watershed

The conversion of isotopic ratios to soil ratios using organic carbon content from the sources is presented in Fig. 4. Results of the stable IsoSource model showed that the soil contribution from the four sources ranged from 3.1 % by eucalyptus field to 37.1 % by road in June 2018 (Fig. 4). However, the order of the proportion of soil contributed by the sources changed in September with sugarcane field having the highest proportion (40.5 %) with the least contribution (2.7 %) from the eucalyptus field. It therefore shows that sugarcane fields, stream channels and roads were the dominant sources of sediment deposited at the watershed outlets with little contribution from eucalyptus fields. Compared to June, the exported soil from the road and eucalyptus field reduced in September by 25.7 and 12.4 %, respectively. The sharp decrease in soil proportion contributed by the road in September might be connected to the repair (pavement) of some of the roads despite highly intense rainfall in September (230 mm) than June (149 mm). In contrast, despite an increase in sugarcane canopy, which reduced the direct impact of raindrops on soil surface, the proportion of exported sediment from sugarcane field increased by 25.2 %. Our previous study demonstrated that the sword-shaped leaf of sugarcane is neither effective in intercepting raindrops nor preventing selective removal of soil under the sugarcane canopy (Li *et al*., 2020c). More precipitation makes it possible for sediment deposited on the slope to be transferred and transported to the water body. Like sugarcane field, the proportion of soil contributed by the stream channel bank increased in September by 6.3 % as compared with June, but decreasing rate. The occurrence of grasses in the stream bank perhaps reduced the amount of erosion and slows down the output and transfer of sediment in the stream channel. However, the little increase in soil proportion by the stream channel bank, in spite of increase in vegetated water ways in September, could be attributed to increase in rainfall as evident from the previous study (Li *et al*., 2020b). Although, the study of Claudio *et al*. (2018) in central Chile showed that seasonality. had no effect on the contribution of sources. However, it is obvious from our study that

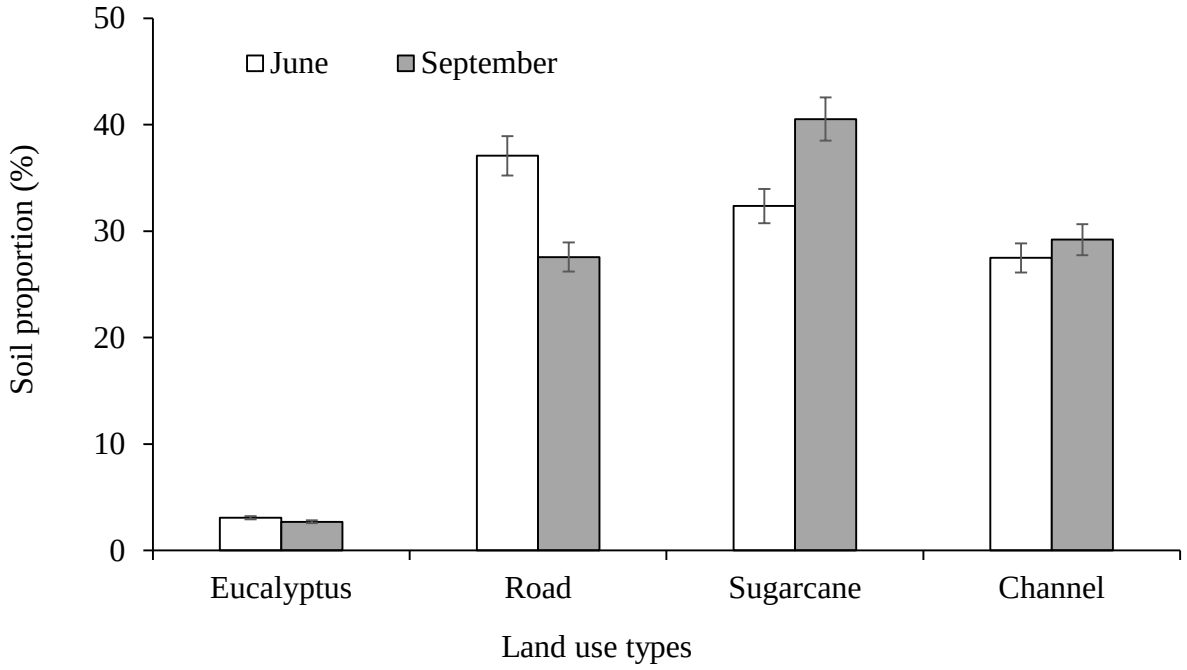

Fig. 4. Soil proportion contributed by different land use types in the study watershed. Error bars on the columns are the standard error at $p \leq 0.05$.

extreme rainfall conditions, such as the hot wet climate zone of southeast China, could influence the proportion of soil contribution from various land use types. It is worth noting that towards September 2018, the southeast China witnessed tropical typhoon and extreme rainfall conditions, which appeared to have significantly influenced the soil contribution from the different sources in the study watershed.

Following the implementation of land integration planning policy in Guangxi Zhuang autonomous region in 2018, some of the eucalyptus fields were replaced with sugarcane (Li, et al., 2020a). The natural river channel was widened, and artificial diversion channels were dug (Li et al., 2020b). These artificial diversion channels reduced the direct flow of surface runoff from the upper reaches to the stream channel to a certain extent, especially on gentle slopes with slopes less than 5°. Mekonnen *et al*. (2015) reported that artificial channels and waterways, such as soil conservation management control, are particularly effective in sediment retention and can significantly reduce sediment load. Meanwhile, the differences in topography and soil type of each land use type dictated the differences in the contributions of watershed sediment sources. Mabit *et al*. (2018) also related sediment sources to their geomorphologic, temporal characteristics, and the distance between them and the sedimentary area in Vienna, northern Austria. For instance, eucalyptus plantations only occupied the upper reaches of the watershed with heavy canopy cover and a distance of more than 1500 m from the outlet of each sub-watershed. These perhaps make the eucalyptus plantation less susceptible to channel erosion is with little soil contribution to the outlets, since it is difficult for the sediment to migrate through such a long distance. Meanwhile, the interception of raindrop by the eucalyptus canopies limited the splashing of surface soil while the speed of runoff could not get the required potential to form many channels unlike other land use types in the watershed. Previous studies have also linked the reduction in surface runoff to vegetation canopy by intercepting the rain droplets from direct hitting of soil surface (Tiecher *et al*., 2017; Cerdà *et al*., 2018).

Sediment and nutrients entering the river from the sources

The total exported sediment and particulate N and P from the entire watershed in summer and autumn 2018 are presented in Table 3. The sediment and particulate N and P loss rates were higher in the summer by 59.4, 106.1, and 37.0%, respectively than in the autumn. In our previous studies at the watershed, we identified rainfall, percentage of ground covered by sugarcane canopy, and fertilizer application time as the main factors causing the variations in the amount of sediment and associated N and P during summer and autumn (Li *et al*., 2020c). However, despite the increase (about 80%) in ground cover and no fertilizer application in September (early autumn), the magnitude of sediment loss increased by 34.5% when compared to June (early summer) following 54.4% increase in rainfall. The loss rates of sediment and particulate N and P contributed by roads, stream channel banks, sugarcane and eucalyptus fields to the outlets in summer and autumn were presented in Fig. 5. The magnitudes of exported sediment in the summer

Table 3: Total sediment and nutrient loads from the entire watershed to the river during summer and autumn in 2018.

Season	Sediment loss ($t\ ha^{-1}$)	STN loss	STP loss
		($kg\ ha^{-1}$)	
Early summer	8.18	14.26	3.09
Late summer	9.90	11.21	4.98
Early autumn	11.00	11.92	5.76
Late autumn	0.34	0.44	0.13

(3.03 and 3.67 t ha^{-1} in early and late summer, respectively) from road surfaces were more than other sources by 0.1–11 times. But in autumn, the magnitudes of export (4.46 and 0.14 t ha^{-1} in early and late autumn, respectively) from sugarcane field dominated, and they were higher than other sources by 0.4–14 times (Fig. 5a). In a similar trend, particulate N and P exports from the watershed were dominated by the road and sugarcane field in summer and autumn, respectively (Figs. 5b and 5c).

Comparing the changes in sediment loss rates from the four sources in June and September, there was no change in sediment loss rate from the road, perhaps due to road amendment and grass cover, but the sediment loss rates increased by 42.7, 16.0, and 68.3% in September from stream channel, eucalyptus, and sugarcane fields, respectively (Fig. 5a). However, while the exported particulate N from the road, stream channel and eucalyptus field decreased by 37.9, 11.2 and 26.8%, respectively, it increased by 4.7% in September compared to June (Fig. 5b). On the other hand, the exported particulate P from the road, stream channel, eucalyptus, and sugarcane fields increased in September as compared to June by 38.6, 98.1, 63.3 and 133.3%, respectively (Fig. 5c). Previous studies have reported that sediment is an important vector for phosphorus transport to waterbodies during erosion processes (Lewis et al., 2013; Li *et al*., 2020c). These studies identified an increase in rainfall and runoff as the main factors increasing particulate P as also observed in our study.

Meanwhile, the entry coefficient of PN and PP (Table 4) showed that the specific quantity of pollutants entering river channels did not have a similar trend as the estimated contributions determined by CSSI. Although the changes in PN and PP between June and September did not follow a discernible trend, the loss of PN and PP through the stream channel had the highest entry coefficients and was closely followed by the road (Table 4). The order of contribution of land use types to NPS pollution, using the entry coefficient, was stream channel > road > sugarcane > eucalyptus. The highest entry coefficient of PN and PP aligns with assertion of Li *et al*. (2020b), who reported a significant contribution of stream channel to NPS pollution in the area, where the stream channel erosion offset 119% N and 40% P of applied fertilizers.

Key factors influencing soil proportions from different land use types

Table 5 shows the loadings for the first two (2) principal components (PCs) of variables (factors) influencing soil proportion from different sources. The PCA showed that the 2 PCs were significant, having eigenvalues of 4.08 and 1.24 for PC1 and PC2, respectively (Table 5). The biplot showed that the total variance explained by PC1 and PC2 were 68.1 and 20.6 %, respectively (Fig. 6), which accounted for a cumulative variance of 88.7 % of the total variation. In this study, soil proportion contributed by the land use types was inversely correlated ($P \leq 0.05$) with SOM, slope gradient, and ground cover, but positively correlated with

Table 4: Specific nutrient rate of diffuse N and P entering the river from land use types

Nutrient	Land use types	Coefficient of entry	
		June 2018	September 2018
PN	Road	0.210	0.138
	Stream Channel	0.273	0.329
	Sugarcane	0.141	0.118
	Eucalyptus	0.046	0.023
PP	Road	0.211	0.161
	Stream Channel	0.271	0.287
	Sugarcane	0.175	0.171
	Eucalyptus	0.055	0.038

Where PP and PN are diffuse particulate nitrogen and phosphorus in the sediment, respectively

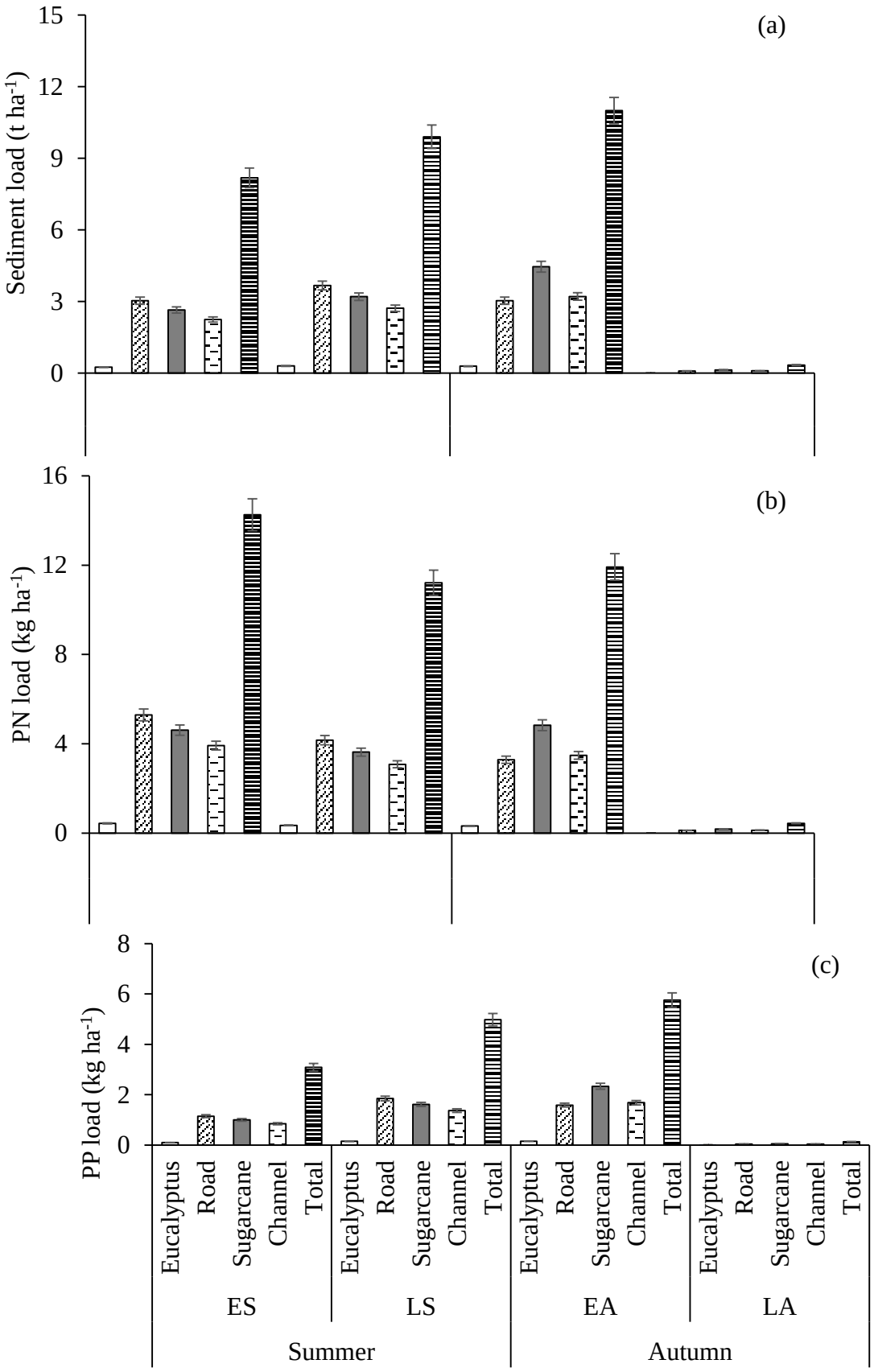

Fig. 5. Variation of sediment and nutrient exports from different land use types in summer and autumn 2018. Error bars on the columns are the standard error at $p \leq 0.05$. Where ES is early summer, LS is late summer, EA is early autumn and LA is late autumn

bulk density (Fig. 6). However, soil proportions had no significant relationships (P >0.05) with soil nitrogen and phosphorus.

The increased level of SOM coupled with vegetation cover in eucalyptus plantations, perhaps reduced significantly the amount of soil proportion exported by soil erosion from the land use. Decrease in soil loss with increased ground cover (Sun *et al*., 2019; Li *et al*., 2020c) and SOM (Conforti *et al*., 2013) have also been reported by previous studies. Increased SOM level stabilizes soil surface by reducing the vulnerability of the soil to erosion (Are *et al*., 2018). The progressive removal of SOM by soil erosion from the newly constructed roads threatened its protecting role, thus enhanced erosion processes in June as compared to September. Meanwhile, routine maintenance of roads, using stone and grass covers prior to CSSI sampling in September, played important role in reducing soil loss from the road. This perhaps led to reduction in soil loss in September than June. However, the increased soil and particulate P losses under sugarcane plantation in

Table 5: Principal component analysis with eigenvalues of factors (variables) influencing soil

Variable	Principal component (PC)	
	PC1	PC2
X1 (Ground cover)	**0.4487**	-0.2005
X2 (Bulk density)	**-0.4592**	0.1807
X3 (Slope)	0.3655	**-0.5228**
X4 (SOM)	**0.4084**	-0.1465
X5 (Soil TN)	0.3975	**0.5291**
X6 (Soil TP)	0.3597	**0.5937**
Eigenvalues	4.08	1.24
Variance (%)	68.1	20.6
Cumulative variance (%)	68.1	88.7

Bold values correspond to variables with high loading rates above 0.4 which are retained for key predictor in PCA analysis. SOM is the soil organic matter, TN is the total nitrogen, and TP is the total phosphorus.

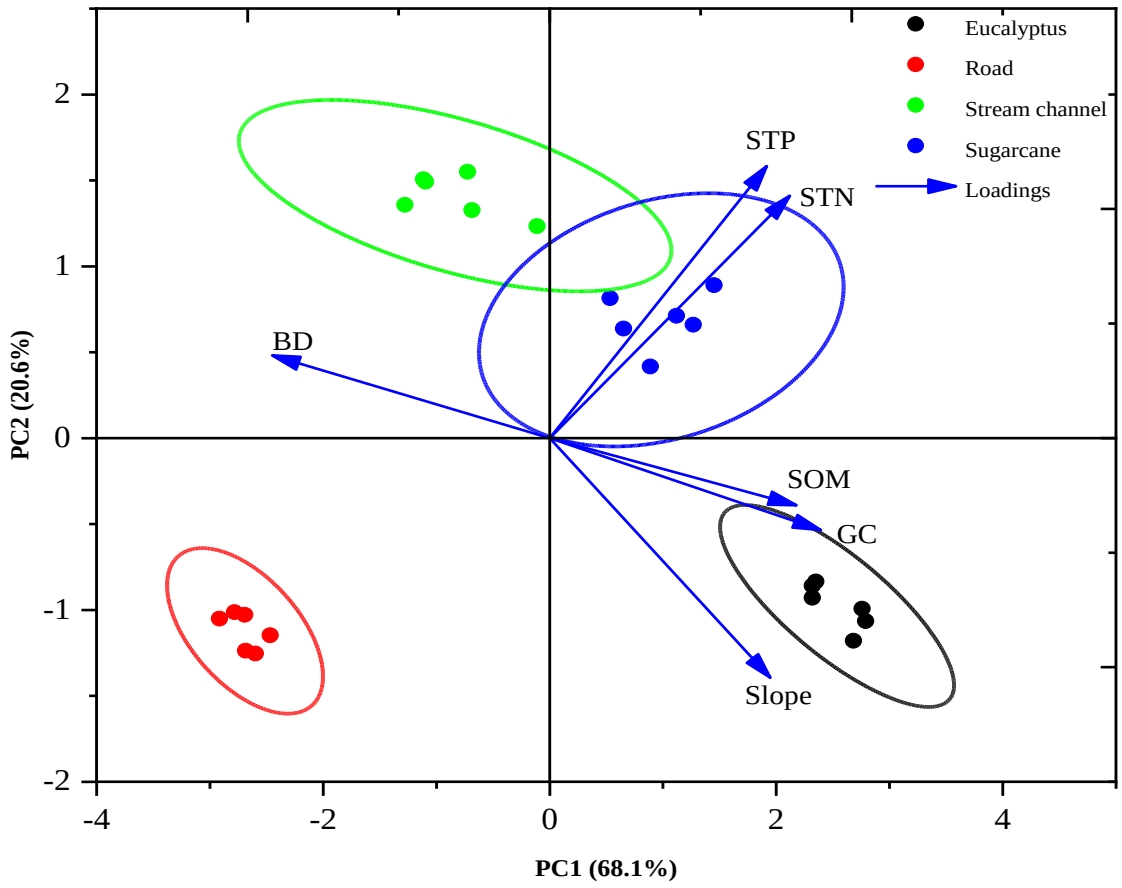

Fig. 6. Principal component analysis (scores and loadings) showing the distribution of the underlying factors as they influence soil proportion

September could be linked to increased rainfall amount and the fact that larger percentage (about 73%) of new sugarcane plants was replanted within 2018 as compared with the ratooned sugarcane of the previous year (Li et al., 2020c). Although, rainfall played important role in increasing the soil loss generally in September as compared to June in all sources, but the effect of increased rainfall was offset by ground cover and SOM in this study. Meanwhile, many studies reported increase in soil loss rates following slope steepness (Liu *et al*., 2015; He *et al*., 2019; Abdalla *et al*. 2019). In this study, the inverse relationship between soil loss and slope gradient could be linked to the fact that the lower slopes of the watershed were occupied by stream channels with increased interconnectivity between roads and stream channels (Li *et al*., 2020a).

Conclusion

We investigated the sources of sediment and measured the entry coefficient of particulate nitrogen (PN) and phosphorus (PP) entering freshwater from land use types. A combine application of isotopic fingerprinting using CSSI and entry coefficient were applied to quantify sediment, PN and PP entering the river from four land use types in June (summer) and September (autumn) 2018. The δ^{13}C-FA value of the mixture showed that only bulk δ^{13}C, FAs C22:0 (Behenic acid), and C24:0 (Lignoceric acid) met the criteria for distinguishing between sediment sources. The magnitude of contribution from different sources to bulk soil δ^{13}C was in the order of road > sugarcane > stream channel > eucalyptus in June, while it was in the order of sugarcane > stream channel > road > eucalyptus in September. The soil proportion contributed to the sediment mixture by the sources followed similar trends in bulk soil δ^{13}C for both June and September. However, the order of contribution of land use types to non-point source (NPS) pollution, using entry coefficient, was stream channel > road > sugarcane > eucalyptus. Increased rainfall in September generally increased the sediment and particulate N and P proportions from the land use types except road, whereas, the entry coefficient in September reduced compare to June except stream channel. The results of the PCA indicated that PC1 and PC2 accounted for a cumulative variance of 88.7 % of total variation in soil proportion from the four land use types. The magnitudes of soil proportion from different sources had significant correlations ($P \leq 0.05$) with ground cover, soil organic matter (SOM), bulk density and slope gradient, but not correlated ((P >0.05) with soil N and P. For a better understanding of sediment redistribution and contributions of land use types to channel erosion and NPS pollution, application of CSSI techniques can accurately predict the specific quantities of soil, PN and PP entering waterbodies from an intensively cultivated land.

Acknowledgements

This work was supported by Science and Technology Major Project of Guangxi (Guike AA17204078) and Base Scientific Technology and Talents Programme (Guike AD17195098).

Reference

Abdalla, K., Dickey, M., Hill, T., and Scott-Shaw, B. (2019). Assessment of soil erosion under rainfed sugarcane in KwaZulu-Natal, South Africa. *Natural Res. Forum* 43: 241–252.

Alewell, C., Birkholz, A., Meusburger, K., Schindler Wildhaber, Y. and Mabit, L. (2016). Quantitative sediment source attribution with compound-specific isotope analysis in a C3 plant-dominated catchment (central Switzerland). *Biogeosciences* 13: 1587–1596.

Are, K.S., Oshunsanya, S.O. and Oluwatosin, G.A. (2018). Changes in soil physical health indicators of an eroded land as influenced by integrated use of narrow grass strips and mulch. *Soil Till. Res*. 184: 269–280.

Borelli, P., Robinson, D.A., Panagos, P., Lugato, E., Yang, J.E., Alewell C., Wuepper, D., Montanarella, L. and Ballabio, C. (2020). Land use and climate change impacts on global soil erosion by water (2015-2070). *PNAS* 117: 21994–22001.

Bravo-Linares, C., Schuller, P., Castillo, A., Ovando-Fuentealba, L., Muñoz-Arcos, E., Alarcón, O, de los Santos-Villalobos, S., Cardoso, R., Muniz, M., Meigikos, dos Anjos, R., Bustamante-Ortega, R. and Dercon, G. (2018). First use of a compound-specific stable isotope (CSSI) technique to trace sediment transport in

upland forest catchments of Chile. *Sci Total Environ*. 618: 1114–1124

Bremner, J.M. (1996). Nitrogen-total. In: Sparks, D.L., Page, A.L., Helmke, P.A., Loeppert, R.H., Soltanpour, P.N., Tabatabai, M.A., Johnston, C.T., Sumner, M.E. (Eds.), Methods of Soil Analysis, Part 3. Soil Science Society of America, Madison, pp. 1085–1121.

Cerdà, A., Rodrigo-Comino, J., Giménez-Morera, A. and Keesstra, S.D. (2018). Hydrological and erosional impact and farmer's perception on catch crops and weeds in citrus organic farming in Canyoles river watershed, Eastern Spain. *Agric. Ecosyst. Environ*. 258: 49–58.

Claudio, B-L., Paulina, S., Alejandra, C., Luis, O-F., Enrique, M-A., Oscar, A., Sergio, de los S-V., Renan, C., Marcelo, M., Roberto, M. dos A., Ramón, B-O. and Gerd, D. 2018. First use of a compound-specific stable isotope (CSSI) technique to trace sediment transport in upland forest catchments of Chile. *Sci. Total Environ*. 618: 1114–1124.

Collins, A.L., Walling, D.E. and Leeks, G.J.L. (1997). Sediment sources in the upper severn catchment: a fingerprinting approach. *Hydrol. Earth Syst. Sci*. 1: 509–521.

Collins, A.L., Pulley, S., Foster, I.D.L., Gellis, A., Porto, P. and Horowitz, A.J. (2017). Sediment source fingerprinting as an aid to catchment management: A review of the current state of knowledge and a methodological decision-tree for end-users. *J. Environ. Manage.* 194: 86–108.

Conforti, M., Buttafuoco, G., Leone, A.P., Aucelli, P.P.C., Robustelli, G. and Scarciglia, F. (2013). Studying the relationship between water-induced soil erosion and soil organic matter using Vis–NIR spectroscopy and geomorphological analysis: A case study in southern Italy. *Catena* 110: 44–58.

Du, P. and Walling, D.E. (2017). Fingerprinting surficial sediment sources: exploring some potential problems associated with the spatial variability of source material properties. *J. Environ. Manag.* 194: 4–15.

Evrard, O., Poulenard, J., Némery, J., Ayrault, S., Gratiot, N., Duvert, C., Prat, C., Lefévre, I., Bonté, P. and Esteves, M. (2013). Tracing sediment sources in a tropical highland catchment of central Mexico by using conventional and alternative fingerprinting methods. *Hydrol. Process*. 27: 911–922.

Gibbs, M.M. (2008). Identifying source soils in contemporary estuarine sediments: a new compound-specific isotope method. *Estuar. Coasts* 31: 344–359.

Gibbs, M.M. (2014). Protocols on the use of Compound-Specific Stable Isotopes to identify and apportion soil sources from land use. Revised 2013. Contract report to Joint FAO/IAEA Division of Nuclear Techniques in Food and Agriculture. Available on line at. http://www-naweb.iaea.org/nafa/swmn/public/CSSI-technique-protocolsrevised-2013.pdf (126 pp).

Glaser, B. (2005). Compound-specific stable-isotope (δ 13 C) analysis in soil science. *J. Plant Nutr. Soil Sci.* 168: 633–648.

Grossman, R.B. and Reinsch, T.G. (2002). Bulk density and linear extensibility: Core method. In: Dane, J.H., Topp, G.C. (Eds.), Methods of Soil Analysis. Part 4. Physical Methods. Soil Science Society of America, Inc., Madison, WI, pp. 208–228.

He, X., Wang, Y., Li, T., He, S., Zheng, Z., Zhang, X., Huang, H., Yu, H., Liu, T. and Lin, C. (2019). Phosphorus losses under heavy rain from the sloping farmlands in the purple hilly region of Southwestern China. *J. Soil. Sed*. 19: 4005–4020.

Jin, Z., Wang, J., Chen, J., Zhang, R., Li, Y., Lu, Y. and He, K. (2020). Identifying the sources of nitrate in a small watershed using $\delta^{15}N$-$\delta^{18}O$ isotopes of nitrate in the Kelan Reservoir, Guangxi, China. *Agric. Ecosyst. Environ*. 297: 106936.

Lewis, C., Rafique, R., Foley, N., Leahy, P., Morgan, G., Albertson, J., Kumar, S. and Kiely, G. (2013). Seasonal exports of phosphorus from intensively fertilised nested grassland catchments. *J. Environ. Sci*. 25(9): 1847–1857.

Li, Y., Are, K.S., Qin, Z., Huang, Z., Abegunrin, T.P., Houssou, A.A., Guo, H., Gu, M. and Wei, L. (2020a). Farmland size increase significantly accelerates road surface rill erosion and nutrient losses in southern subtropics of China. *Soil Till. Res*. 204: 104689.

Li, Y., Tang, C., Huang, Z., Hussain, Z., Are, K.S., Abegunrin, T.P., Qin, Z. and Guo, H. (2020b). Increase in farm size significantly accelerated stream channel erosion and associated nutrient losses from an intensive agricultural watershed. *Agric. Ecosyst. Environ*. 295: 106900.

Li, Y., Are, K.S., Huang, Z., Guo, H., Wei, L., Abegunrin, T.P., Gu, M. and Qin, Z. (2020c). Particulate N and P exports from sugarcane growing watershed are more influenced by surface runoff than fertilization. *Agric. Ecosyst. Environ*. 302: 107083.

Li, Y., Mo, Y., Are, K.S., Huang, Z., Guo, H., Tang, C., Abegunrin, T.P., Qin, Z., Kang., Z. and Wang, X. (2021). Sugarcane planting patterns control ephemeral gully erosion and associated nutrient losses: Evidence from hillslope observation. *Agric. Ecosyst. Environ*. 309: 107289.

Liu, D., She, D., Yu, S., Shao, G. and Chen, D. (2015). Rainfall intensity and slope gradient effects on sediment losses and splash from a saline-sodic soil under coastal reclamation. *Catena* 128: 54–62.

Mabit, L., Gibbs, M., Mbaye, M., Mesusburger, K., Toloza, A., Resch, C., Klik, A., Swales, A. and Alewell, C. (2018). Novel application of Compound Specific Stable Isotope (CSSI) techniques to investigate on-site sediment origins across arable fields. *Geoderma* 316: 19–26.

Mekonnen, M., Keesstra, S.D., Stroosnijder, L., Baartman, J.E.M. and Maroulis, J. (2015). Soil conservation through sediment trapping: a review. *Land Degrad. Dev*. 26 (6): 544–556.

Phillips, D.L. and Gregg, J.W. (2001). Uncertainty in source partitioning using stable isotopes. *Oecologia* 127: 171–179.

Phillips D.L. and Gregg J.W. 2003. Source partitioning using stable isotopes: coping with too many sources. *Oecologia*, 136: 261–269.

Recanatesi, F., Ripa, M.N., Leone, A., Luigi, P. and Luca, S. (2013). Land Use, Climate and Transport of Nutrients: Evidence Emerging from the Lake Vicocase Study. *Environ. Manage*. 52: 503–513.

Reiffarth, D.G., Petticrew, E.L., Owens, P.N. and Lobb, D.A. (2016). Sources of variability in fatty acid (FA) biomarkers in the application of compound-specific stable isotopes (CSSIs) to soil and sediment fingerprinting and tracing: A review. *Sci. Total Environ*. 565: 8-27.

Reiffarth, D.G., Petticrew, E.L., Owens, P.N. and Lobb, D.A. (2019). Spatial differentiation of cultivated soils using compound-specific stable isotopes (CSSIs) in a temperate agricultural watershed in Manitoba, Canada. *J. Soil. Sed*. 19: 3411–3426.

Rodriguez-Blanco, M.L., Taboada-Castro, M.M. and Taboada-Castro, M.T. ()2010. Sediment and phosphorus loss in runoff from an agroforestry catchment, NW Spain. *Land Degrad. Develop*. 21: 161–170.

Sommers, L.E. and Nelson, D.W. (1972). Determination of total phosphorus in soils: a rapid perchloric acid digestion procedure. *Soil Sci. Soc. Am. Proc*. 36: 902–904

Sun, W., Mu, X., Gao, P., Zhao, G., Li, J., Zhang, Y. and Francis, C. (2019). Landscape patches influencing hillslope erosion processes and flow hydrodynamics. *Geoderma* 353: 391–400.

Swales, A. and Gibbs, M.M. (2020). Transition in the isotopic signatures of fatty-acid soil biomarkers under changing land use: Insights from a multi-decadal chronosequence. *Sci. Total Environ*. 722: 137850.

Tiecher, T., Minella, J.P.G., Caner, L., Evrard, O., Zafar, M., Capoane, V., Le Gall, M. and Rheinheimer dos Santos, D. (2017). Quantifying land use contributions to suspended sediment in a large cultivated catchment of Southern Brazil (Guaporé River, Rio Grande do Sul). *Agric. Ecosyst. Environ*. 237: 95–108.

Tolosa, I., Fiorini, S., Gasser, B., Martin, J. and Miquel, J.C. (2013). Carbon sources in suspended particles and surface sediments from the Beaufort Sea revealed by molecular lipid biomarkers and compound-specific isotope analysis. *Biogeosciences* 10: 2061–2087.

Upadhayay, H.R., Bodé, S., Griepentrog, M., Huygens, D., Bajracharya, R.M., Blake, W.H., Dercon, G., Mabit, L., Gibbs, M., Semmens, B.X., Stock, B.C., Cornelis, W. and Boeckx, P. (2017). Methodological

perspectives on the application of compound-specific stable isotope fingerprinting for sediment source apportionment. *J. Soils Sediments* 17 (6): 1537–1553.

Walling, D.E. (2005). Tracing suspended sediment sources in catchments and river systems. *Sci. Total Environ*. 344: 159–184.

Walling, D.E., Collins, A.L. and Stroud, R.W. (2008). Tracing suspended sediment and particulate phosphorus sources in catchments. *J. Hydrol*. 350: 274–289.

Zhou, M., Deng, J., Lin, Y., Belete, M., Wang, K., Comber, A., Huang, L. and Gan, M. (2019). Identifying the effects of land use change on sediment export: Integrating sediment source and sediment delivery in the Qiantang River Basin, China. *Sci. Total Environ*. 686: 38–49.